Characterization of coherent population-trapping resonances as atomic frequency references

Svenja Knappe and Robert Wynands

Institut für Angewandte Physik, Universität Bonn, Wegelerstrasse 8, D-53115 Bonn, Germany

John Kitching, Hugh G. Robinson, and Leo Hollberg

Time and Frequency Division, Mail Stop 847.10, National Institute of Standards and Technology, 325 Broadway, Boulder, Colorado 80303

Received November 23, 2000; revised manuscript received April 3, 2001

A low-cost, potentially compact and robust microwave frequency reference can be constructed by use of vertical-cavity surface-emitting lasers and coherent population-trapping resonances in Cs vapor cells. Fractional frequency instabilities of $2 \times 10^{-11}/\sqrt{\tau/\mathrm{s}}$ have been achieved with a minimum of 7×10^{-13} at $\tau = 1000$ s. The performance of this device as a function of external parameters such as light intensity, optical detuning, and cell temperature is discussed. The dependence of the dark-line resonance signal on these parameters can be understood largely by means of a simple, three-level model. The short-term stability depends critically on the optical detuning, whereas the long-term stability is limited currently by line shifts due to drifts in cell temperature.

OCIS codes: 270.1670, 020.1670, 020.3690, 300.6320, 300.6420, 120.3930.

1. INTRODUCTION

In the SI system of units the second is defined by the magnetic dipole transition between the $|F = 3,\ m = 0\rangle$ and $|F = 4,\ m = 0\rangle$ ground-state Zeeman components of the Cs atom. The traditional way of constructing an atomic clock is with a Cs atomic beam, excited by a 9.2-GHz microwave field in two Ramsey interaction zones.[1] Recently, advanced laser cooling techniques have made possible the construction of "fountain clocks," where a cloud of cold atoms is launched against gravity, resulting in long interaction times and narrow linewidths.[2–5] Both designs, however, are bulky and experimentally complex, and the accuracies they provide are much higher than that required for many applications. Over the years, several alternative techniques have been investigated, such as optically pumped microwave double resonances,[6–8] Raman scattering,[9] and coherent population-trapping (CPT) resonances.[10–15] Relatively compact and inexpensive frequency references are available commercially that use lamp-pumped alkali-vapor cells and external microwave fields to probe the clock transitions.[1] Applications such as global-positioning system receivers and in-field telecommunication devices require compact, low-cost frequency references with fractional frequency instabilities better than 10^{-11} over one day, a performance level that is difficult to reach with quartz crystals. Important additional specifications here concern cost, size, robustness, and low power consumption,[16] none of which can be met with atomic beams or fountains.

Due to their linewidths, CPT resonances have been under consideration as frequency references for many years.[7,17–19] These resonances can be excited in a Λ configuration, where coherence is induced between two long-lived ground states by coupling them to a common excited state by two laser fields with a stable relative phase. If the difference frequency of the two light fields is exactly equal to the splitting between the two lower states, the atoms can be pumped into a coherent superposition of these two states, the coherent dark state, which no longer couples to the excited state. The absorption of light is reduced, resulting in electromagnetically induced transparency. Using the Cs D_2 line, for example, Λ systems can be formed with the hyperfine components $F = 3$ and 4 of the $6S_{1/2}$ ground state and the hyperfine-split excited states $6P_{3/2}$, $F' = 3$ and 4. Such a CPT resonance absorption signal is shown in Fig. 1, where the detector voltage is normalized to the value at maximum Doppler absorption. The difference frequency between the two optical fields is varied near the ground state's hyperfine splitting of 9.2 GHz, and the total laser power transmitted through the cell is monitored. Although the absorption is changed by only 0.15%, the resulting Q factors (the ratio of resonance frequency to resonance width) are greater than 2×10^8, since linewidths of <50 Hz are possible at a good signal-to-noise ratio.[20]

Recent progress in the field of vertical-cavity surface-emitting lasers (VCSELs) allows for their use in vapor-cell frequency references as compact, reliable, easy-to-handle light sources with low power consumption. Their high modulation bandwidth makes them suitable for a compact and robust device based on CPT resonances. The required bichromatic field can be produced by direct modulation of the injection current. Reliable single-mode VCSELs at 852 nm are becoming available commercially, allowing excitation of the D_2 line of Cs.

In this paper we will discuss the dependence of the resonance on important experimental parameters. The frequency stability of the clock is expressed by the Allan

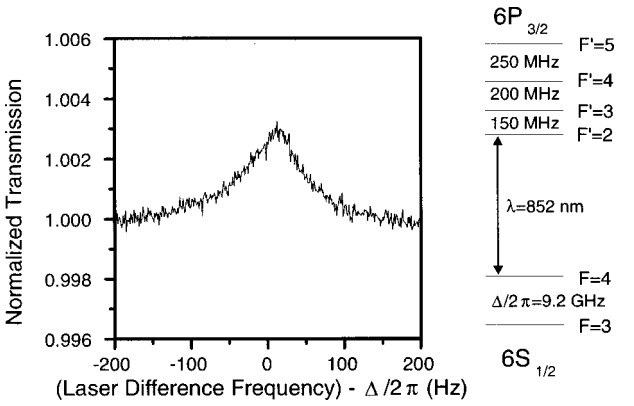

Fig. 1. Left: Spectrum of the dark-resonance absorption signal with dc detection of the laser power transmitted through the cell, normalized to the maximum absorbed power. Right: Level diagram of the Cs D_2 line. Λ systems can be formed with the ground states and the excited states $F' = 3$ and 4.

deviation.[21] The short-term stability is found to be determined by frequency fluctuations of the laser translated into amplitude noise on the detector by the slope of the Doppler-broadened background absorption line, whereas the long-term stability depends mainly on slow frequency drifts. To optimize the clock design, it is helpful to understand the underlying physics that influences the CPT resonance signal.

For short averaging times the performance of the clock depends directly on the slope of the resonance signal, given by its height and its width. The height and width of the signal are discussed separately because while the width is determined by the lifetime of the ground-state coherence, the height depends also on the number of atoms populating the dark state, aspects that are not necessarily coupled. The clock is then operated at the point where the slope divided by the noise amplitude is at its maximum. In addition to the slope of the error signal at the operating point, the performance of the clock is limited by frequency shifts resulting from either a change in the shape of the resonance, which might shift the lock point, or shifts of the resonance peak itself as the external parameters change. Although the accuracy of the clock is not the main concern for the compact setup discussed here, its frequency should be reproducible and stable, and line shifts would adversely affect the long-term performance. Understanding systematic shifts will help to overcome the clock's sensitivity to environmental parameters. In order to find the optimum operating values for the frequency reference, the influence of important parameters such as optical detuning, laser intensity, cell temperature, RF power, and modulation frequencies was studied. The first three will be discussed in detail in the following sections. The last two parameters are not very interesting in the context of this paper because their influence is strongly dependent on the specific details of the mechanical and electrical setup. For instance, the modulation frequencies for the servo loops were chosen well away from electrical interference peaks, whereas the power of the gigahertz modulation of the laser current has to be chosen such that the fraction of the optical power transferred into the first-order modulation sidebands is maximum, given the bad RF transmission of the commercial TO package of the VCSEL.

2. SIMPLE MODEL OF COHERENT POPULATION TRAPPING

The shape of the coherent population-trapping resonance can be derived analytically from a density-matrix calculation for a simple three-level system consisting of two ground states $|1\rangle$ and $|2\rangle$ separated by an energy $\hbar\Delta$ and a single excited state $|3\rangle$ (see Fig. 2). When two light fields with frequencies ω_1 and ω_2 couple the ground states to the excited state, atoms can populate a superposition state[22]

$$|\mathrm{NC}\rangle \propto g_1|2\rangle - g_2 \exp(-i\Delta t)|1\rangle, \tag{1}$$

where g_1 and g_2 are the Rabi frequencies of the two transitions. This state is not coupled to the excited state by the applied bichromatic field if the difference frequency of the two fields is equal to the ground-state splitting ($\omega_2 - \omega_1 = \Delta$). Due to optical pumping, atoms will accumulate in the dark state, where they cannot absorb light. Tuning the difference frequency $\omega_2 - \omega_1$ will result in a narrow resonance with a width given by the lifetime of the noncoupled state $|\mathrm{NC}\rangle$, which can in principle be relatively long.

For a simple symmetric three-level model ($g_1 = g_2 = g$), density-matrix calculations predict for a single atom at rest that in the case of resonant, low-intensity light fields[23] the resonance will be Lorentzian with a width

$$\gamma_{\mathrm{CPT}} = 2\Gamma_{12} + \frac{g^2}{\Gamma}, \tag{2}$$

which depends on the relaxation rates of the ground- and excited-state coherence, Γ_{12} and Γ, respectively. Since the upper ground state of Cs has a lifetime of several thousand years, the experimental width is limited by other broadening factors, such as the relative phase stability of the two laser fields, residual Doppler and time-of-flight broadening, collisional broadening, and saturation broadening. In the same low-intensity limit the height of the dark-line resonance H is given by the number of atoms populating the dark state[23]:

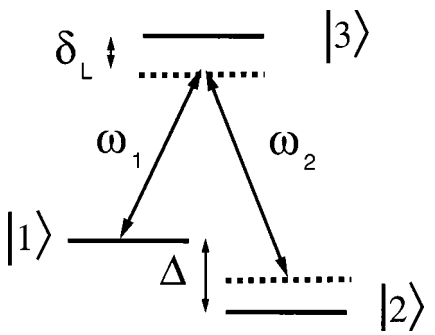

Fig. 2. Three-level scheme used to model the CPT resonances. The optical detuning δ_L and the detuning from the dark-line resonance in this diagram are negative.

$$H \propto n_{\mathrm{Cs}} \frac{g^4}{\Gamma^3} \frac{1}{2\Gamma_{12} + g^2/\Gamma}. \tag{3}$$

Here n_{Cs} is the number density of Cs atoms in the vapor. In the case of an ideal three-level system, darkness will be complete if the intensity is high enough. A real atom such as Cs is more complicated, especially because of the excited-state hyperfine structure shown in Fig. 1: in general, two Λ systems can be formed for each pair of ground-state Zeeman components, one by coupling to the $F' = 3$, and another by coupling to the $F' = 4$ state. The dark state $|\mathrm{NC}\rangle$ depends on the coupling strengths of the two transitions involved. For the two excited states of cesium these coupling strengths are different; thus the dark state for one is not completely dark for the other. The overall transition probability is therefore not exactly zero. On the D_2 line there are, in addition, the excited $F' = 2$ and 5 states that couple to one ground state only. Atoms in the dark state can still be excited by one-photon transitions to these states, reducing the height and increasing the width of the CPT resonance.[24]

Furthermore, a dark state can be populated only with those atoms contained in the pair of ground-state Zeeman levels for which the resonance condition is fulfilled. In a real experiment, all Zeeman levels are populated about equally, so that only one eight of the cesium atoms contribute to the CPT resonance signal, whereas all atoms account for the large Doppler background. Overall, this results in a resonance height of typically only 1.5% of the Doppler absorption signal, corresponding to an increase in transmitted power of only 0.15% for our 2-cm-long cell at room temperature. Although the Cs atom is really a 48-level system on the D_2 line, the calculations with a three-level model agree surprisingly well with the measurements. Nevertheless, it will be shown that the hyperfine structure of the excited state cannot be completely neglected.[24]

3. EXPERIMENTAL CONFIGURATION

In the experiment an oxide-confined VCSEL is used, with a threshold current of 0.82 mA at 31.2 °C and a linewidth of approximately 50 MHz, emitting 870 μW in a single spatial and spectral mode at 852 nm. The linearly polarized output from the VCSEL is sent through a quarter-wave plate to create a circular polarization and is attenuated by neutral-density filters, leaving ~10 μW in a beam 4 mm in diameter at the entrance to the vapor cell (see Fig. 3). To create a bichromatic light field with a difference frequency of 9.2 GHz, the VCSEL's injection current is modulated at 4.6 GHz, half the ground-state hyperfine splitting of Cs. This is done with 12.6 mW of RF power synthesized from a 5-MHz crystal oscillator. The two first-order sidebands are then used to excite the resonance. The light is sent through a Cs vapor cell 2 cm long and 2.5 cm in diameter. A photodiode detects the transmitted power. The laser is tuned such that the two first-order sidebands are resonant with the transitions from the two $6S_{1/2}$ ground-state components to the excited $6P_{3/2}$ state. Due to the large tuning rates of the laser frequency with injection current and temperature (of the order of −300 GHz/mA and −25 GHz/K), the laser current and temperature must be carefully controlled. The laser is locked to the center of the Doppler-broadened optical resonance line by sinusoidally modulating its current at 10 kHz, followed by demodulation of the absorption signal on the photodiode with a lock-in amplifier and finally a servo amplifier that feeds back a correction signal onto the injection current.

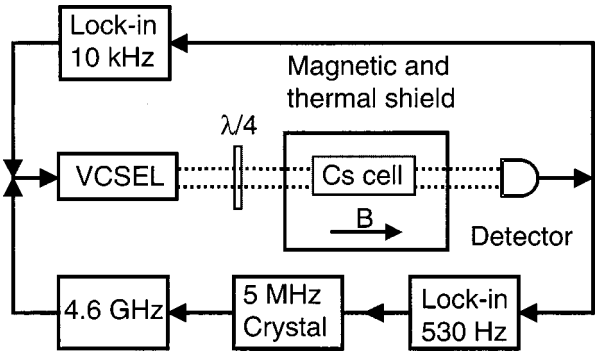

Fig. 3. Experimental setup of the compact dark-resonance Cs clock. The 4.6-GHz signal modulates the laser injection current to produce two sidebands separated by 9.2 GHz, which probe the dark-line resonance in the Cs cell. The lock-in at 10 kHz is used to lock the laser to the Cs resonance, and the lock-in at 530 Hz is used to lock the 5-MHz quartz crystal that in turn controls the frequency of the 4.6-GHz source.

A second servo-loop locks the RF modulator to the dark-resonance signal. This is done by modulating the 5-MHz reference crystal for the synthesizer at 530 Hz and detecting in turn the resulting modulation that appears on the optical power transmitted through the cell. Phase-modulation indices as high as 0.7 were obtained with these parameters. The resulting frequency-modulation spectrum consists of dispersive Lorentzians at the line center and at the positions of the 530-Hz modulation sidebands. The distance between the maximum and the minimum of each of the dispersive Lorentzians, i.e., the full width at half-maximum (FWHM) of the corresponding absorptive Lorentzian (the dark line), is ~100 Hz typically. The Cs vapor cell is thermally isolated and temperature stabilized to within 100 μK of 32 °C. It sits inside a mu-metal shield that reduces stray transverse magnetic fields by a factor of ~2000. To isolate the dark resonance on the $m_3 = 0 \leftrightarrow m_4 = 0$ Zeeman component, a small homogeneous longitudinal magnetic field of 10-μT flux density is applied. Neon at a pressure of 9.7 kPa was added to the Cs vapor to reduce transit time and Doppler effects. While the CPT resonance is narrowed compared with the case of pure Cs vapor, the optical resonance is broadened by 86-MHz/kPa Ne.[25] This means that the homogeneous width of the optical transition exceeds the laser linewidth. In addition, the CPT resonance frequency is shifted upward by ~46 kHz by Cs–Ne collisions at this pressure.[20]

Because of the large modulation bandwidth of the VCSELs (~6 GHz) the fraction of optical power transferred to the first-order sidebands is near its maximum even for moderate RF power. With 12.6 mW of RF power injected into the laser, 47% and 19% of the optical power are transferred to the blue and red first-order sidebands, respectively, leaving only 8% in the carrier. The remaining power is in the sidebands of higher order. The sideband

asymmetry can be explained by additional amplitude modulation when the laser current is modulated.

With the RF modulation applied, the laser is locked to the position of maximum optical absorption, and the 4.6-GHz frequency is scanned over the dark-line resonance. The dark-line height and width are recovered by fitting the error signal with an FM lineshape of a Lorentzian line.[26] In addition, the 4.6-GHz signal can be locked to the resonance by feeding an error-signal voltage to the tuning port on the quartz crystal of reference. The thus-stabilized 4.6-GHz signal is then compared with the signal from a hydrogen maser. In this way the frequency of the reference can be measured as a function of time and its stability optimized through appropriate choices of experimental parameters. RF power, beam diameter, buffer-gas pressure, and modulation frequencies and indices for the two servo loops are chosen to obtain the optimal signal-to-noise ratio. In the following sections we will discuss the clock's performance when varying the laser intensity, the optical detuning, and the cell temperature. Note that all frequencies and frequency shifts will be referred to the full 9.2-GHz hyperfine frequency.

4. LASER INTENSITY

The performance of the clock was investigated as a function of laser intensity. The overall intensity of the laser was attenuated with a neutral-density filter in front of the cell; the relative power in the blue and the red first-order sidebands remained constant. A large beam diameter, here 4 mm, enables operation at low intensities while still maintaining enough laser power to overcome the electronic noise in the detection circuit. This choice of diameter is determined by magnetic-field inhomogeneities as well as the size of the cell for a small device. The noise at the detector's output was measured at the modulation frequency of 530 Hz and found to increase linearly with intensity because it is strongly dominated by laser frequency noise combined with frequency-dependent absorption.[15] The noise approaches a constant value as the intensity goes to zero, where it is dominated by electronic noise.

To understand the dependence of the dark-resonance signal on intensity, the width and height have been extracted from a fit to the error signal and are plotted separately in Figs. 4 and 5 (squares) as a function of the total intensity contained in the two first-order sidebands. It can be seen from Fig. 4 that the width increases linearly with intensity I by $G/\Gamma = 5.6\,\mathrm{Hz}/(\mu\mathrm{W/cm}^2)$ (with $g^2 = GI$), from a minimum width of $2\Gamma_{12} = 117\,\mathrm{Hz}$ at zero intensity (solid line). For this buffer-gas pressure the finite width in the zero-intensity limit is a result mainly of collisions between Cs and Ne atoms.[27] The observed linear increase of the width with intensity can be a result of power broadening, as it appears explicitly in Eq. (2). On the other hand, the single-photon transition rate to the excited states $F' = 2$ and 5 should be proportional to the intensity, as well. This increases the ground-state dephasing Γ_{12} and therefore results in a linear broadening of the dark-line resonance with laser intensity. This broadening rate G/Γ is reduced with higher buffer-gas pressures as the optical transition is broadened.

Relation (3) predicts the amplitude of the dark-line signal to increase quadratically with intensity I for $I < \Gamma_{12}\Gamma/G \approx 20\,\mu\mathrm{W/cm}^2$ and to increase proportionally to I for higher intensities. This can be seen in Fig. 5, where the height of the dark resonance is shown as a function of the resonant intensity in front of the cell. The squares are the measured values, and the solid curve is relation (3) plotted for the parameter values determined from slope and offset in a plot like Fig. 4. This shows that for zero optical detuning, the dark-resonance line shape agrees quite well with the predictions of the symmetric three-level model in the low-intensity region.

The frequency of the center of the dark-line resonance as a function of resonant light intensity incident on the cell is plotted in Fig. 6. The observed shift is mainly due to the ac Stark shift because other effects like an intensity-dependent change in the slope of the 800-MHz-wide optical absorption line are completely negligible on the scale of the 100-Hz-wide dark-resonance line. For an ideal three-level system with no decay of the ground-state coherence, no light shift is expected. But since the resonance in the real Cs atom is not completely dark, light shifts caused by all excited states are expected. Whereas the Stark shift from a monochromatic light field in a two-level atom is linear in intensity, the one measured for this

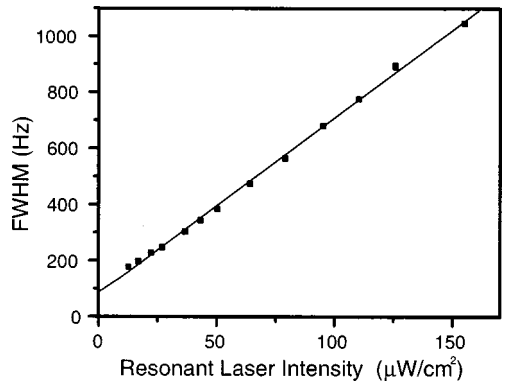

Fig. 4. Full width of the dark-resonance error signal measured at 1-kHz modulation frequency as a function of the laser intensity contained in the two first-order sidebands incident on the cell (squares). The solid line is a fit of Eq. (2).

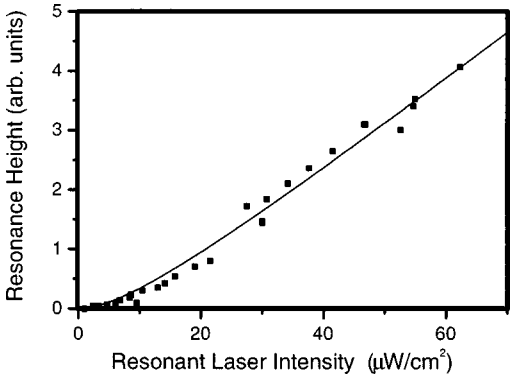

Fig. 5. Height of the dark-resonance error signal measured in a 2-cm cell containing 5.1-kPa neon as a function of the laser intensity contained in the two first-order sidebands incident on the cell. The squares are the measured values, and the solid curve is relation (3) plotted for the parameter values determined from slope and offset in a plot like Fig. 4.

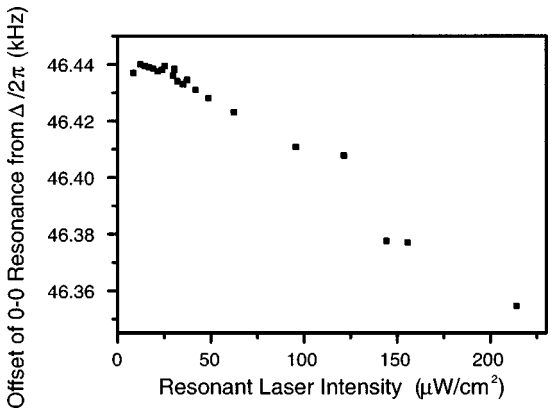

Fig. 6. Frequency shift of the 0–0 resonance from the unperturbed ground-state hyperfine frequency as a function of total laser intensity, measured under the locked condition and compared with a hydrogen maser reference.

system shows some deviation from linear behavior at low intensities.[28] This nonlinearity could come about because the light shift depends on the interaction strength of the light field with the transitions: this transition strength changes on Raman resonance, giving rise to a deviation from the linear shift. So the overall shift on the D_2 line is not just the weighted sum of the six contributing single-photon transitions to the various excited states. Calculating the light shifts for the dark state is rather complicated, especially when modeling a real atom where more than one excited level exists. For the linear region a shift rate of approximately ~500 Hz/(mW/cm^2) is measured. This result agrees with the data in Ref. 28. Use of even higher buffer-gas pressures suppresses the light shifts even further because the transition rates drop due to collisional dephasing. We have not investigated intensity-dependent modulation-related drifts,[1] believing them to be small as compared with buffer-gas-related temperature drifts (see below).

To summarize, the optimum operating point for the clock is at an intensity just above that for which the constant noise contributions from the electronics become important, but for which the light shift is as small as possible, ~60 μW/cm^2 in our case.

5. OPTICAL DETUNING

When the 4.6-GHz modulation is present, creating sidebands on the laser, and the laser frequency is tuned slowly over the optical transition, the resulting absorption profile is a superposition of the transitions from ground state $F = 3$ to the hyperfine components $F' = 2,3,4$ and from the ground state $F = 4$ to $F' = 3,4,5$. The Doppler-broadened transitions are further broadened homogeneously by Cs–Ne collisions, resulting in an optical absorption profile with a full width of 1.3 GHz. The optical detuning, δ_L, is the deviation of the laser frequency from the peak absorption. The absorption is a function of the power in the two sidebands at ±4.6 GHz, whereas the laser carrier and the higher-order sidebands are not absorbed. For a total laser intensity of 45 μW/cm^2 the dark-line resonance signal and the noise on the signal were measured as a function of δ_L. It was found that the Allan deviation of the 4.6-GHz signal when the system is locked is determined mainly by the noise resulting from laser frequency fluctuations, which noise shows a distinct minimum at $\delta_L = -40$ MHz. This noise is plotted in Fig. 7 and is normalized to the dc voltage on the detector, that is, the optical power.

The solid curve in the plot is the calculated noise level when the detector's electronic noise and the laser's intensity and frequency noise are taken into account.[15] With a laser linewidth of 50 MHz, the laser's frequency noise dominates the noise on the detected signal if the laser is tuned to the side of the optical-resonance line. The frequency fluctuations are translated into intensity fluctuations on the detector by the slope of this optical resonance. The fact that the minimum of the noise is shifted to $\delta_L = -40$ MHz is due to the dependence of the optical hyperfine pumping on the Fourier frequency of the noise. We have investigated this effect in detail, as reported elsewhere;[29] only a brief description will be given here. When the shape of the optical-absorption profile is probed by frequency-modulated light (like, e.g., the frequency noise of the laser), it is found to be different for modulation frequencies below or above the optical hyperfine pumping rate. For slow modulation the relative populations of the two hyperfine ground states can adjust to the changing excitation probabilities due to the changing laser frequencies, but for higher modulation frequencies the populations cannot follow this variation. This process mainly leads to a shift of the high-frequency optical-absorption profile but is also accompanied by a small amount of additional noise that further increases the noise minimum; this excess noise was, however, not considered in the calculation of the solid curve in Fig. 7.

The change of noise level as a function of optical detuning is the most decisive factor in determining the short-term frequency stability of the system. However, the height and the width of the dark-resonance signal also change. The resonance height and width were measured as a function of laser detuning at a constant intensity; the results are plotted in Figs. 8 and 9. It is remarkable that over a detuning range of 700 MHz the height of the resonance varies by a factor of 2, whereas the width does not change much. To understand this difference in behavior

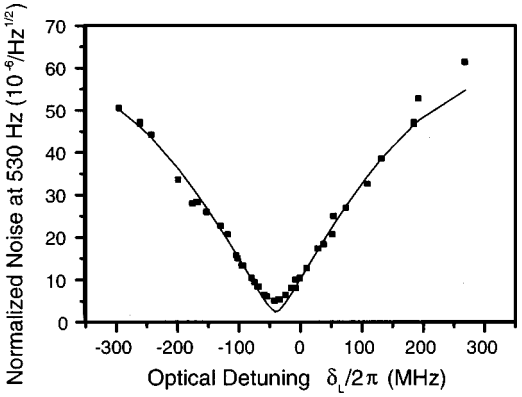

Fig. 7. Power spectral density at 530 Hz as a function of the optical detuning δ_L, normalized to the power on the detector (squares). The solid curve in the plot is the calculated noise level when the detector's electronic noise and the laser's intensity and frequency noise are taken into account.[15]

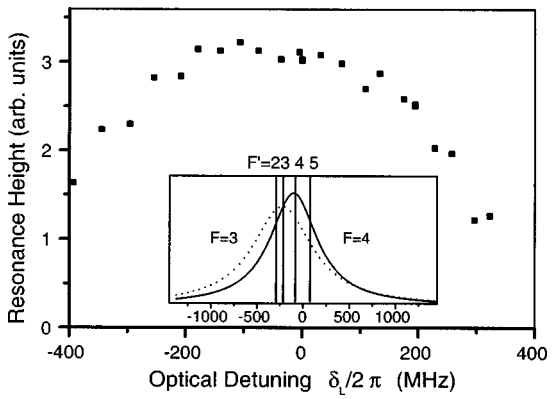

Fig. 8. Measured amplitude of the dark-resonance error signal as a function of optical detuning δ_L taken for a total resonant laser intensity of 45 μW/cm^2 and 9.7 kPa of Ne. The inset shows fitted curves for the amplitude of the dark line for data from Ref. 24 taken for a laser intensity of 0.97 mW/cm^2 and 7.2 kPa of Ne. The vertical lines show the position of the excited state's hyperfine levels.

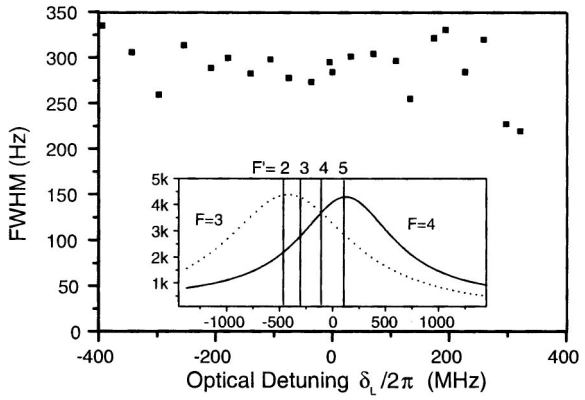

Fig. 9. Full width at half-maximum of the dark-resonance error signal as a function of optical detuning δ_L taken for a total resonant laser intensity of 45 μW/cm^2 and 9.7-kPa Ne. The inset shows curves fitted to the data of Ref. 24 taken for a laser intensity of 0.97 mW/cm^2 and 7.2 kPa of Ne. The vertical lines show the position of the excited state's hyperfine levels.

qualitatively it is instructive to look at cases where one of the two laser fields is much stronger than the other (e.g., by a factor of 65).[24]

The amplitude of the dark resonance reaches its maximum value when the two-photon transition probability is maximum. In a hypothetical three-level system, this occurs when both lasers are resonant with the excited state, since the dark state has to be populated by optical pumping. The existence of two suitable excited states complicates the situation. For the asymmetric case of Ref. 24 with the strong laser field on the transition from the $F = 4$ ground state, the two-photon transition probability is largest when the fields are in resonance with the $F' = 4$ excited state. The transition dominates the transition to the $F' = 3$ state by a factor of 7 due to coupling coefficients. The CPT resonance signal therefore reaches its maximum value when the optical fields are in resonance with the $F' = 4$ state. The inset to Fig. 8 shows the curves fitted to the height of the dark-line resonance in this asymmetric case, taken from Ref. 24. We observe that the height (solid curve) reaches its maximum at a laser detuning where the strong field is resonant with the transition from $F = 4$ to $F' = 4$, indicated by the second vertical line from the right.

For the opposite case of a strong carrier on the $F = 3$ ground state the excited states $F' = 3$ and $F' = 4$ contribute with a ratio of 5:2, causing the resonance to be highest with the fields tuned closer to the $F' = 3$ state (dotted curve). If the two sidebands are of nearly equal strength, as in the experiments described here, a superposition of both cases is expected, since the two-photon transition amplitude increases when the laser is in resonance with either the $F' = 3$ or 4 state. This results in a somewhat broader range of laser tuning that gives a nearly constant amplitude of the dark-line resonance as shown in Fig. 8.

In contrast, the width of the dark-line resonance (Fig. 9) is dominated by the excitation of atoms out of the dark state to the excited $F' = 2$ and 5 states, which do not contribute to a dark state but serve rather as loss channels. These one-photon transitions decrease the lifetime of the ground-state coherence. Again, looking at the two limiting cases of one very intense laser field and one of lesser intensity, the maximum width occurs when the intense carrier field is resonant with the $F = 4$ to $F' = 5$ transition. Similarly for the reversed intensity ratio, the width peaks when the intense laser field is tuned to the $F = 3 \leftrightarrow F' = 2$ transition. This can be seen in the inset to Fig. 9, which shows the fit curves to the width of the dark-line resonance in this asymmetric case (taken from Ref. 24). Once again, for two fields of equal strength, tuning to either the $F' = 2$ or the $F' = 5$ level increases the one-photon transition rates, resulting in a broad pedestal for the width, with a shape given roughly by the sum of the two curves in the inset.

In summary, we find that the amplitude of the dark-line resonance does not depend strongly on the detuning, whereas the background noise has a pronounced minimum at a laser detuning of ~ -40 MHz from the maximum of the absorption. This choice of detuning maximizes the signal-to-noise ratio for the operation of the frequency reference.[15] The laser's frequency can be stabilized to this point without much difficulty.

Changing the optical detuning not only changes the shape of the resonance signal but also shifts the frequency of the resonance. The line shift with optical detuning is the result of ac Stark shifts from the excited state's loss channels. This can be seen in the inset of Fig. 10, which shows the two extremely unbalanced cases in terms of laser power.[24] The net shift as a function of optical detuning has a dispersive shape, reversing its sign when interchanging the transition with which the strong field is near-resonant. The point of inflection coincides with the transitions to the excited $F' = 2$ or 5 states when the strong carrier is on the $F = 3$ or 4 state, respectively.

Using two laser fields of nearly equal strength (as in our experiment here), the shifts should partly cancel. The overall shift in this configuration is $\sim$60 times smaller: we measured a shift of $\sim$20 mHz/MHz at its maximum for a total laser intensity of 45μW/cm^2. Part of this reduction, however, is simply due to the lower laser intensity here (a factor of 20 as opposed to that in Ref. 24)

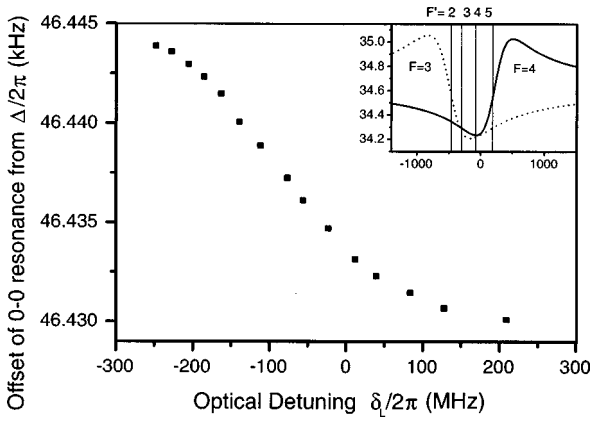

Fig. 10. Measured frequency shift of the 0–0 resonance from the unperturbed ground state's hyperfine frequency as a function of optical detuning δ_L, taken for a total resonant laser intensity of 45 μW/cm^2 and 9.7 kPa of Ne. The inset shows curves fitted to the data of Ref. 24 taken for a laser intensity of 0.97 mW/cm^2 and 7.2 kPa of Ne.

and a higher buffer-gas pressure (a factor of 1.3). Operating on the D_1 instead of the D_2 line might reduce these shifts and simultaneously increase the slope of the signal because no excited states are present that couple to a single ground state only.

6. CELL TEMPERATURE

The Cs cell is enclosed in a thermal shield containing small holes for the laser beam. The temperature of the cell was stabilized to within ~0.1 mK by use of a thermistor attached to the outside of the cell wall. The shape of the dark-line resonance was observed for different cell temperatures between 20 °C and 65 °C. The amplitude of the dark-line resonance is plotted in Fig. 11 as a function of cell temperature. The amplitude reaches its maximum value at cell temperatures of ~33 °C and drops rapidly with higher temperatures, disappearing completely at >55 °C.

To understand this behavior, we note that the amplitude of the resonance is proportional to the number of Cs atoms in the dark state [relation (3)], of which the number in turn depends on the atom density in the vapor. This dependence can be seen for the lower-temperature regions in Fig. 11. As the number of Cs atoms in the vapor is increased further, more light is absorbed by those atoms not in the dark state. At temperatures near 50 °C the cell becomes optically thick; thus essentially no resonant light reaches the detector. This increasing optical thickness makes the resonance disappear quickly at >40 °C for a cell 2 cm in length. The dependence of the dark-line resonance on cell temperature is in qualitative agreement with the predictions of a simple model based on the increase in Cs atoms in the vapor, as described above. Use of a shorter cell shifts the temperature of the maximum of the dark-line resonance amplitude to higher temperatures.[30] This could be desirable in a compact, low-power setup that might need to be operated at temperatures up to 85 °C. It is preferable to stabilize the cell above the ambient temperature so that only heating is required, as opposed to both cooling and heating; this results in a more power-efficient system. Although the height of the resonance depends strongly on the cell temperature, its width remains nearly constant, within 50 Hz.

Over the temperature range of 20 to 50 °C the noise at the lock-in frequency of 530 Hz was also measured. The noise stays fairly constant over this temperature range, decreasing slightly for higher temperatures as the slope of the FM–AM conversion gets shallower and as the amount of light on the detector decreases. Despite the complete absorption of the first-order sidebands at high temperatures, approximately one third of the optical power is contained in the other sidebands and passes through the cell to the detector. We found that for our experimental system (and for averaging times less than ~1000 s) we obtained the best results for cell temperatures of ~30 °C.

Although the cell is thermally isolated and temperature stabilized, residual temperature drifts still limit the long-term stability of the frequency reference. A linear shift rate with temperature of 10 Hz/K at 9.2 GHz for 9.7 kPa of neon was measured in the range between 25 °C and 50 °C. This is consistent with the measurements for direct microwave excitation of the 0–0 resonance.[31] For temperature instabilities less than 100μK this shift would cause frequency instabilities in the 10^{-13} region, far below the measured values for long times. The residual temperature dependence that limits the Allan deviation could be caused by insufficient temperature stabilization of the cell windows. We observed a correlation between the room temperature and the center frequency of the dark-line resonance, even though the temperature sensor near the center of the cell did not show any residual temperature fluctuations.

The addition of other buffer-gas species can shift the resonance in the opposite direction as a function of temperature. For example, we made Cs cells with a mixture of neon and argon and observed that the temperature-dependent shift was reduced to <0.4 Hz/K. This improved the long-term stability of the clock significantly, as shown in Fig. 12. However, there was some degradation of the short-term stability in the mixed-gas cell, due to additional broadening of the resonance line. Figure 12 shows a typical Allan deviation for the tabletop setup described in Section 3 with a 2-cm cell containing 9.7-kPa neon (solid squares). Although the use of a 5.3-kPa

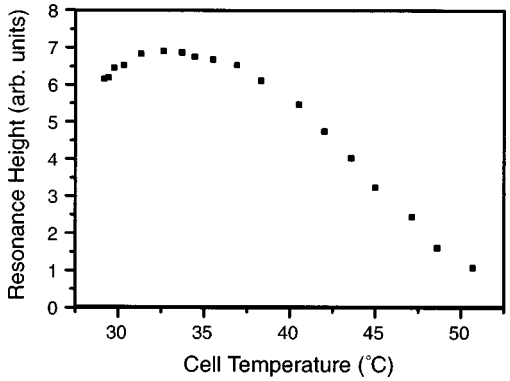

Fig. 11. Measured amplitude of the dark-resonance error signal as a function of cell temperature.

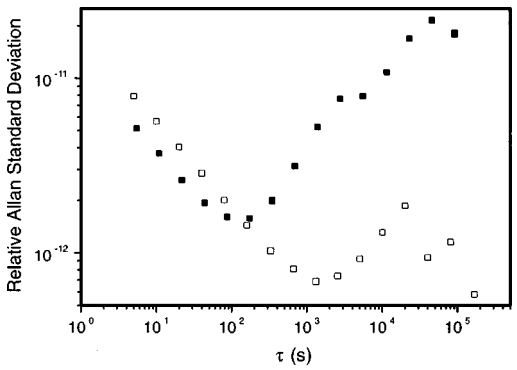

Fig. 12. Allan deviation of the 4.6-GHz signal as a function of averaging time τ, when locked as measured for the tabletop setup with a cell containing 9.7 kPa of neon (filled squares) or 5.3 kPa of a Ne–Ar mixture (open squares). The mixed gas cell has a lower temperature dependence of the frequency of the dark-line resonance and hence better stability for larger times. This is at the expense of somewhat worse stability of short times.

Ne–Ar buffer gas mixture degraded the short-term stability of the clock by a factor of 2, due to a broader resonance line, the long-term stability improved, as shown by the open squares in the same plot. With this mixture of buffer gases, Allan deviations of $2 \times 10^{-11}/\sqrt{\tau/s}$, dropping to 7×10^{-13} at 1000 s, were achieved.

7. CONCLUSION

A compact and robust low-cost frequency reference has been studied with regard to optimizing external parameters such as laser intensity, optical detuning, and cell temperature. The dependence of the clock performance on these environmental parameters is consistent with the predictions of a simple model for the resonance signal. We believe it is possible to design this device into a physics package of less than 20-cm^3 volume and with an electrical power consumption of $<$100 mW. Since this design does not contain deformable parts such as microwave cavities, it should maintain its performance even under acceleration.

Further investigations could include improvements of the long-term stability, currently limited by temperature-induced drifts, investigations of acceleration sensitivity, and miniaturization. Limitations in the availability of VCSELs at 894 nm make it currently difficult to improve the short-term stability by probing the resonance on the D_1 line of Cs. The D_1 line has the advantage of a simplified hyperfine structure in the excited state, such that Λ systems are allowed with all excited states. This should increase the overall amplitude of the dark-line resonance and reduce its width by prolonging the lifetime of the dark state. Light shifts should be reduced as well. Furthermore, it should be possible to operate the clock at higher temperatures because the single-photon absorption is more strongly suppressed, and therefore the optical thickness for a given temperature is reduced. An alternative may be to use Rb vapor instead, where some VCSELs are available at the D_1 wavelength. However, as of now these laser diodes seem to be much less reliable than the ones operating at 852 nm. Rb has an additional advantage over Cs, in that the vapor cells can be heated to higher temperatures before reaching vapor pressures where spin-exchange collisions become important, making operation of the clocks at higher temperature possible.

REFERENCES

1. J. Vanier and C. Audoin, *The Quantum Physics of Atomic Frequency Standards* (Hilger, London, 1989).
2. J. R. Zacharias, unpublished (1953), described in N. F. Ramsey, "Nobel lecture: experiments with separated oscillatory fields and hydrogen masers," Rev. Mod. Phys. **62**, 541 (1990).
3. M. Kasevich, E. Riis, S. Chu, and R. De Voe, "Rf spectroscopy in an atomic fountain," Phys. Rev. Lett. **63**, 612–615 (1989).
4. A. Clairon, P. Laurent, G. Santarelli, S. Ghezali, S. Lea, and M. Bahoura, "A cesium fountain frequency standard: preliminary results," IEEE Trans. Instrum. Meas. **44**, 128–131 (1995).
5. D. Meekhof, S. R. Jefferts, M. Stepanovic, and T. Parker, "Accuracy evaluation of a cesium fountain primary frequency standard at NIST," IEEE Trans. Instrum. Meas. **50**, 507–509 (2001).
6. M. Poelker, P. Kumar, and S.-T. Hoe, "Laser frequency translation: a new method," Opt. Lett. **16**, 1853–1855 (1991).
7. P. Kumar and J. H. Shapiro, "Observation of Raman-shifted oscillation near the sodium *D* lines," Opt. Lett. **10**, 226–228 (1985).
8. C. Rahman and H. G. Robison, "Rb 0–0 hyperfine transition in evacuated wall-coated cell at melting temperature," IEEE J. Quantum Electron. **QE-23**, 452–454 (1987).
9. N. Vukičević, A. S. Zibrov, L. Hollberg, F. L. Walls, J. Kitching, and H. G. Robinson, "Compact diode-laser based rubidium frequency reference," IEEE Trans. Ultrason. Ferroelectr. Freq. Control **47**, 1122–1126 (2000).
10. P. R. Hemmer, M. S. Shahriar, H. Lamela-Rivera, S. P. Smith, B. E. Bernacki, and S. Ezekiel, "Semiconductor laser excitation of Ramsey fringes by using a Raman transition in a cesium beam," J. Opt. Soc. Am. B **10**, 1326–1329 (1993).
11. N. Cry, M. Têtu, and M. Breton, "All-optical microwave frequency standard: a proposal," IEEE Trans. Instrum. Meas. **42**, 640–649 (1993).
12. J. Vanier, A. Godone, and F. Levi, "Coherent microwave emission in cesium under coherent population trapping," Phys. Rev. A **59**, R12–R15 (1999).
13. F. Levi, A. Godone, and J. Vanier, "The light shift effect in the coherent population trapping cesium maser," IEEE Trans. Ultrason. Ferroelectr. Freq. Control **46**, 609–615 (1999).
14. A. Godone, F. Levi, and J. Vanier, "Coherent microwave emission without population inversion: a new atomic frequency standard," IEEE Trans. Instrum. Meas. **48**, 504–507 (1999).
15. J. Kitching, S. Knappe, N. Vukičević, L. Hollberg, R. Wynands, and W. Weidemann, "A microwave frequency reference based on VCSEL-driven dark line resonances in Cs vapor," IEEE Trans. Instrum. Meas. **49**, 1313–1317 (2000).
16. J. A. Kusters and C. A. Adams, "Performance requirements of communication base station time standards," RF Design (May 1999), pp. 28–38.
17. J. E. Thomas, S. Ezekiel, C. C. Leiby, Jr., R. N. Picard, and C. R. Willis, "Ultrahigh-resolution spectroscopy and frequency standards in the microwave and far-infrared regions using optical lasers," Opt. Lett. **6**, 298–300 (1981).
18. J. E. Thomas, P. R. Hemmer, S. Ezekiel, C. C. Leiby, Jr., R. N. Picard, and C. R. Willis, "Observation of Ramsey fringes using a stimulated, resonance Raman transition in a sodium atomic beam," Phys. Rev. Lett. **48**, 867–870 (1982).
19. P. R. Hemmer, S. Ezekiel, and C. C. Leiby, Jr., "Stabilization

of a microwave oscillator using a resonance Raman transition in a sodium beam," Opt. Lett. **8**, 440–442 (1983).
20. S. Brandt, A. Nagel, R. Wynands, and D. Meschede, "Buffer-gas induced linewidth reduction of coherent dark resonances to below 50 Hz," Phys. Rev. A **56**, R1063–R1066 (1997).
21. J. Barnes, A. Chi, L. Cutler, D. Healey, D. Leeson, T. McGunigal, J. Mullen, W. Smith, R. Sydnor, R. Vessot, and G. Winkler, "Characterization of frequency stability," IEEE Trans. Instrum. Meas. **IM-20**, 105–120 (1971).
22. E. Arimondo, "Relaxation processes in coherent population trapping," Phys. Rev. A **54**, 2216–2223 (1996).
23. J. Vanier, A. Godone, and F. Levi, "Coherent population trapping in cesium: dark lines and coherent microwave emission," Phys. Rev. A **58**, 2345–2358 (1998).
24. A. Nagel, C. Affolderbach, S. Knappe, and R. Wynands, "Influence of excited state hyperfine structure on ground state coherence," Phys. Rev. A **61**, 012504 (2000).
25. N. Allard and J. Kielkopf, "The effect of neutral nonresonant collisions on atomic spectral lines," Rev. Mod. Phys. **54**, 1103–1182 (1982).
26. G. C. Bjorklund, M. D. Levenson, W. Lenth, and C. Ortiz, "Frequency modulation (FM) spectroscopy," Appl. Phys. B **32**, 145–152 (1983).
27. W. Happer, "Optical pumping," Rev. Mod. Phys. **44**, 169–243 (1972).
28. A. Nagel, S. Brandt, D. Meschede, and R. Wynands, "Light shift of coherent population trapping resonances," Europhys. Lett. **48**, 385–389 (1999).
29. J. Kitching, L. Hollberg, S. Knappe, and R. Wynands, "Frequency-dependent optical pumping in atomic Λ systems," Opt. Lett. (to be published).
30. S. Knappe, Institute für Angeuwandte Physik, Universität Bonn, Weglestrasse 8, D-53115 Bonn, Germany; J. Kitching and L. Hollberg, Time and Frequency Division, Mail Stop 847.10, National Institute of Standards and Technology, 325 Broadway, Boulder, Colorado 80303 (personal communication, 2000).
31. N. Beverini, F. Strumia, and G. Rovera, "Buffer gas pressure shifts in the $m_F = 0 \leftrightarrow m_F = 0$ ground state hyperfine line in Cs," Opt. Commun. **37**, 394–396 (1981).